Electron-Spin-Echo Envelope Modulation*

L. G. ROWAN† AND E. L. HAHN
Physics Department, University of California, Berkeley, California
AND
W. B. MIMS
Bell Telephone Laboratories, New York, New York
(Received 20 July 1964)

If an electron-spin moment is reoriented by a pulse of microwave power at magnetic resonance in a time short compared to the Larmor periods of neighboring nuclear moments in a solid, the nuclei suffer nonadiabatic changes in local dipolar field produced by the electron spin. After the pulse, a given nucleus will precess about a new axis of quantization which is appreciably tilted from its original axis if the electron dipolar field at the nuclear site has an appreciable component perpendicular to an applied external magnetic field. Consequently, a coherent oscillating nuclear dipolar field at the electron site modulates the electron Larmor frequency at the lower nuclear resonance frequencies of the nuclear neighbor. The depth of the beat modulation, as it affects the electron free-precession signal, is determined by the magnitude of electron-nuclear magnetic coupling and the extent to which the new axis of nuclear quantization is tilted from its original axis after the microwave pulse. The electron free-precession beats are measured conveniently in terms of the electron-spin-echo envelope modulation pattern obtained from the two-pulse echo experiment. The theory of the effect is developed for purely magnetically coupled nuclei and is confirmed by electron-spin-echo measurements of paramagnetic Ce^{3+} in $CaWO_4$, where the 14%-abundant W^{183} nuclear isotope is coupled to Ce^{3+}. The electron-nuclear ligand tensor dipole-dipole interaction is estimated from experiment to be as much as four times greater than that expected from the point dipole-dipole interaction, and the ligand hyperfine interaction appears to be small.

I. INTRODUCTION

IN electron-nuclear double-resonance (ENDOR) experiments,[1] spin transitions induced by radio-frequency excitation at nuclear magnetic resonance (NMR) frequencies are indicated by a change in the amplitude of the electron spin resonance (EPR) signal. A sensitive detection scheme for NMR transitions and the determination of ligand nuclear hyperfine and dipolar coupling with the electron is therefore available. We present in this paper the theory and experiment of a transient electron-nuclear coupling effect,[2–4] first found by Mims *et al.*,[2] which provides information similar to that of the ENDOR method. By the transient method the electron-spin echo is obtained and the echo envelope exhibits amplitude beat modulation which contains periods corresponding to the NMR frequencies of nuclei which are coupled to the electrons. The strength of the coupling determines the depth of the echo envelope modulation. An external NMR double-resonance excitation required by ENDOR is not necessary in the echo method, but a virtual nuclear double-resonance effect does occur in the echo experiment because of the sudden pulsed reorientation of the electron spins. A sudden change in the direction of the local fields produced at neighboring nuclear sites by the electrons is imposed by EPR microwave pulses in a time short compared to the nuclear Larmor period. If the electron dipolar field is a reasonable fraction of the total precession field at the site of the nucleus, and if this field is not in the direction of the externally applied field, the nucleus will precess coherently about a different axis of quantization immediately after an EPR pulse. This is equivalent to the onset of oscillating NMR transitions as seen from the reference frame of the electron spins. Consequently, oscillations of nuclear dipolar fields at electron sites produce interferences among superposed Zeeman electron states, and coherent electron-echo-envelope modulations appear within times much shorter than the phase decoherence nuclear spin-spin relaxation times. No excess Boltzmann population of nuclear spins is required. The analysis of this effect and its confirmation by experiment is reminiscent of the complicated beat patterns displayed by nuclear echoes in indirect spin-spin coupled systems in liquids where the exchange parameter J exists.[5] The ENDOR method has the advantage that a single nuclear transition of a specific set of equivalent nuclear neighbors can be excited and displayed, whereas the electron-echo method has as its chief disadvantage that all close neighboring nuclei, regardless of their resonant frequencies, will contribute to the envelope pattern. The echo pattern must be carefully analyzed and interpreted in order to infer the individual resonance frequencies. In spite of these disadvantages, there is

* Work supported by the U. S. Office of Naval Research and the National Science Foundation.
† Submitted in partial fulfillment of the requirements for degree of Doctor of Philosophy. Present address: Physics Department, University of North Carolina, Chapel Hill, North Carolina.
[1] G. Feher, Phys. Rev. 114, 1219 (1959).
[2] W. B. Mims, K. Nassau, and J. D. McGee, Phys. Rev. 123, 2059 (1961); J. A. Cowen and D. A. Kaplan, *ibid.* 124, 1098 (1961).
[3] D. A. Kaplan, M. E. Browne, and J. A. Cowen, Rev. Sci. Instr. 32, 1182 (1961).
[4] L. G. Rowan and E. L. Hahn, Bull. Am. Phys. Soc. 8, 592 (1963).
[5] E. L. Hahn and D. E. Maxwell, Phys. Rev. 88, 1070 (1952).

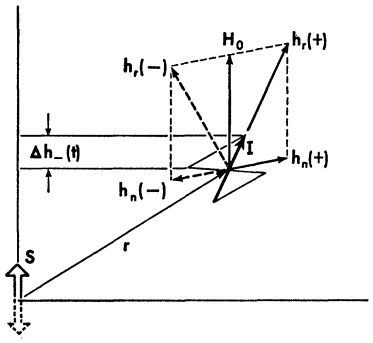

FIG. 1. Dipolar interaction configuration of electron spin S and nuclear spin I placed in the external field H_0. The local field $\mathbf{h}_n(+)$ produced by S up at the site of I switches to $\mathbf{h}_n(-)$ after S is suddenly reversed in direction by an EPR pulse. The resultant nuclear precession field $\mathbf{h}_r(+)$ switches correspondingly to $\mathbf{h}_r(-)$, and the precession of I about $\mathbf{h}_r(-)$ imposes an oscillating local field $\Delta\mathbf{h}(t)$ at the site of S.

evidence in cases where weak nuclear moments are to be detected, and where electron spin-spin diffusion relaxation times are short, that the electron pulse method is more sensitive than the ENDOR method if the electron echoes are reasonably strong.

In this paper, the theory of the experiment is confirmed in detail by the experimental echo beats observed[4] in Ce^{3+} doped $CaWO_4$ single crystals, where the Ce^{3+} ions are coupled with the 14% abundant tungsten (W^{183}) nuclear moments.

II. THEORY

Simple Model

A qualitative picture of the echo modulation effect is obtained from an inspection of Fig. 1. A nuclear spin **I** is placed at a point **r** from an electron spin **S**, and a constant magnetic field $\mathbf{H}_0$ is applied. Each spin produces a dipole field at the site of the other. For a distance $r\approx 3$ Å, the electron field at the nucleus is given by $h_n\approx\mu_e/r^3\approx 1000$ G, and the nuclear field at the electron is given by $h_e\approx\mu_n/r^3\approx 1$ G. With a field $H_0\approx 3000$ G, the electron moment orientations $\pm\boldsymbol{\mu}_e$ give rise to corresponding electron dipole fields $\pm\mathbf{h}_n$, which combine with H_0 to give effective nuclear precession fields $\mathbf{h}_r(\pm)=\mathbf{H}_0\pm\mathbf{h}_n$. [In Fig. 1 $\mathbf{h}_n(\pm)$ corresponds to $\pm\mathbf{h}_n$.] If the EPR microwave pulse turns over an electron spin in the short time

$$t_w\ll 2\pi/\gamma_n|\mathbf{H}_0\pm\mathbf{h}_n|\,,$$

where γ_n is the nuclear gyromagnetic ratio, then the sudden field changes $\pm\mathbf{h}_n\rightarrow\mp\mathbf{h}_n$ take place, corresponding, respectively, to whether the electron orientations are initially $+\boldsymbol{\mu}_e$ or $-\boldsymbol{\mu}_e$. Resultant precession fields at the nuclei will abruptly transform as $\mathbf{h}_r(\pm)\rightarrow\mathbf{h}_r(\mp)$. The nuclei cannot adiabatically follow the new directions into which $\mathbf{h}_r(\mp)$ point, and therefore one set of nuclei will precess in a cone about $\mathbf{h}_r(+)$, and the other set will precess in a cone about $\mathbf{h}_r(-)$, at Larmor frequencies $\gamma_n|\mathbf{h}_r(+)|$ and $\gamma_n|\mathbf{h}_r(-)|$, respectively. Oscillating components $\Delta h_+(t)$ and $\Delta h_-(t)$ of the nuclear dipole fields at the electron sites add in the direction of H_0, where $\Delta h_\pm(t)$ is determined by the difference between the maximum and minimum projections of the nuclear dipole fields along the electron z axis of quantization. Excursions in electron Larmor frequency modulation occur by the amounts $\gamma_e\Delta h_-(t)$ and $\gamma_e\Delta h_-(t)$, each having an oscillatory behavior determined by the nuclear Larmor frequencies $\gamma_n|\mathbf{h}_r(+)|$ and $\gamma_n|\mathbf{h}_r(-)|$, respectively. After a 90° pulse, the electron free precession signal would display interference beats between these nuclear frequencies. In experimental practice, the free precession signal from the electrons is not observed for reasons due to the receiver saturation; instead, the spin-echo signal is observed at $t=\tau$ after the application of a second microwave 180° pulse at time τ. The phase relations of the precessing electrons as indicated in the calculation to follow, give rise to interference effects not only after a 90° pulse, but also in the echo amplitude, depending upon the time τ.

It is evident that the electron beat effect can only occur here if $\Delta h_\pm(t)$ is nonzero; namely, when in the presence of H_0, the nuclear and electron spins have different axes of quantization. Each magnetic state of the total system must be a mixed state. As the field H_0 is decreased to make H_0 comparable to $|h_n|$, then $\Delta h_\pm(t)$ increases and the depth of the modulation pattern is therefore increased. In the limit $H_0<|h_n|$, $H_0\rightarrow 0$, the modulation diminishes toward zero, although the electrons may remain quantized along the direction of an internal crystalline Stark field.[6] In this case, for nuclei coupled only to the electron dipole magnetic field, a change in the $\mathbf{h}_n$ direction does not produce any $\Delta h_\pm(t)$ field at the electron sites.

The Hamiltonian

The quantum-mechanical calculation of the echo envelope begins by assuming a Hamiltonian that represents an electron spin S and a nuclear spin I coupled as an isolated pair in a crystal. The Hamiltonian has the form[7]

$$\mathcal{H}_T=\beta\mathbf{H}_0\cdot\mathbf{g}\cdot\mathbf{S}-\beta_n g_n\mathbf{H}_0\cdot\mathbf{I}+\alpha\mathbf{I}\cdot\mathbf{g}\cdot\mathbf{S}+(\beta\beta_n g_n\rho/r^5)[3(\mathbf{r}\cdot\mathbf{g}\cdot\mathbf{S})(\mathbf{r}\cdot\mathbf{I})-r^2\mathbf{I}\cdot\mathbf{g}\cdot\mathbf{S}],\quad(1)$$

where β and β_n are the electron and nuclear Bohr magneton, respectively; g_n is the nuclear g factor; $\mathbf{g}$ is the electron g tensor which depends on the orientation of the magnetic field H_0 with respect to the crystal axes; and $\mathbf{r}$ is the position vector of the nuclear spin with respect to the electron spin. The first two terms in the

[6] D. E. Kaplan, Bull. Am. Phys. Soc. 8, 468 (1963).
[7] W. Low, in *Solid State Physics*, edited by F. Seitz and D. Turnbull (Academic Press Inc., New York, 1960), Suppl. 2, p. 96.

Hamiltonian pertain to the Zeeman coupling of the electron and nuclear spins to the external magnetic field H_0. The effect of the crystal field is accounted for by the tensor character of the g factor of the electron. In the case of Ce^{3+} doped $CaWO_4$, the crystal field has tetragonal symmetry which gives rise to a $g_{\parallel}$ along the C axis of the crystal and a $g_{\perp}$ perpendicular to the C axis as the diagonal and only components of the tensor. The third term is the isotropic hyperfine coupling energy while the last term arises from direct dipole-dipole and pseudodipole anisotropic hyperfine interactions. The effect of covalent bonding which leads to these interactions with the ligand nucleus is discussed by Marshall and others.[7,8] The constants α and $\rho-1$ are determined by the experiment. The anisotropic hyperfine interaction is introduced by $\rho-1$ which adds to the direct dipolar contribution, where $\rho\geq 1$.[9] We have neglected the coupling of the paramagnetic electron with its own nucleus by assuming a zero spin state of the nucleus.

The Hamiltonian of Eq. (1) can be put in a simpler form by letting the field H_0 and the crystal C axis of symmetry lie in the xz plane, where the C axis is in the z direction. Following a series of rotation transformations,[10] the transformed Hamiltonian for our echo calculation becomes

$$\mathcal{H}=\hbar\omega_e S_z-\hbar\omega_n I_z+\hbar A S_z I_z+\hbar B S_z I_x, \tag{2}$$

where $\hbar\omega_e=g\beta H_0$,

$$g^2=g_{\parallel}^2\cos^2\theta_0+g_{\perp}^2\sin^2\theta_0,$$

$$\hbar\omega_n=g_n\beta_n H_0,$$

$$\hbar A=(gg_n\beta_n\beta\rho/r^3)[(3/g^2)(g_{\parallel}^2\cos\theta_0\cos\theta_I+g_{\perp}^2\sin\theta_0\times\sin\theta_I\cos\varphi_I)(\cos\theta_0\cos\theta_I+\sin\theta_0\sin\theta_I\cos\varphi_I)+(\alpha r^3/g_n\beta_n\beta\rho)-1],$$

$$B^2=B'^2+C'^2,$$

$$\hbar B'=\left(\frac{gg_n\beta_n\beta\rho}{r^3}\right)\left[\left(\frac{3}{g^2}\right)(g_{\parallel}^2\cos\theta_0\cos\theta_I+g_{\perp}^2\sin\theta_0\sin\theta_I\times\sin\varphi_I)(\cos\theta_0\sin\theta_I\cos\varphi_I-\sin\theta_0\cos\varphi_I)+\left(\frac{\alpha r^3}{g_n\beta_n\beta\rho}-1\right)\left(\frac{g_{\perp}^2-g_{\parallel}^2}{g^2}\right)\sin\theta_0\cos\theta_0\right],$$

$$\hbar C'=\left(\frac{gg_n\beta_n\beta\rho}{r^3}\right)\left[\left(\frac{3}{g^2}\right)(g_{\parallel}^2\cos\theta_0\cos\theta_I+g_{\perp}^2\sin\theta_0\times\sin\theta_I\cos\varphi_I)(\sin\theta_I\sin\varphi_I)\right].$$

In the above relations, θ_0 is the angle between the applied field H_0 and the crystal z axis, θ_I is the polar angle between the z or C axis of the crystal and position vector $\mathbf{r}$ to the nuclear spin I, and φ_I is the azimuthal angle about the z axis between the xz plane which contains the field H_0 and the position vector $\mathbf{r}$. The tetragonal symmetry of the crystal field gives rise to the constants $g_{\parallel}$ and $g_{\perp}$, which accounts for the θ_0 dependence of the electron Larmor frequency ω_e in the case of Ce^{3+} in $CaWO_4$. The largest term in $\mathcal{H}$ is $\hbar\omega_e S_z$, and coupling terms which involve S_x and S_y have nonsecular high-frequency variations of the order of ω_e which are therefore omitted.

The eigenvalues of the Hamiltonian $\mathcal{H}$ are easily obtained in a representation in which S_z and I_z are diagonal. Since $\mathcal{H}$ is already diagonal with respect to S_z, we may consider each electron Zeeman level $S_z=m_s$ separately. The Hamiltonian is then written as

$$\mathcal{H}=\hbar\omega_e m_S+\hbar(Am_S-\omega_n)I_z+Bm_S I_x \tag{3}$$

$$=\exp(-i\varphi I_y)[\hbar\omega_e m_S+\hbar K I_z]\exp(i\varphi I_y), \tag{4}$$

where $R(\varphi)=\exp(-i\varphi I_y)$ performs a unitary rotation about the I_y axis. A new Hamiltonian is obtained,

$$\mathcal{H}^*=\exp(i\varphi I_y)\mathcal{H}\exp(-i\varphi I_y) \tag{5}$$

$$=\hbar\omega_e m_S+\hbar K I_z, \tag{6}$$

where

$$K=[(Am_S-\omega_n)^2+B^2m_S^2]^{1/2}, \tag{7}$$

and $\tan\varphi=Bm_S/(Am_S-\omega_n)$. For $m_S=\pm\frac{1}{2}$, $K^{\pm}$ and $\tan\varphi^{\pm}$ are defined accordingly where K^+ and K^- are the nuclear resonance frequencies for the two possible orientations $m_S=\pm\frac{1}{2}$ of the electron spin. The eigenvalues of $\mathcal{H}^*$ are

$$E_{m_I}(m_S)=\hbar\omega_e m_S+\hbar K m_I$$

and the eigenvectors are

$$[\exp i\varphi I_y]|m_S,m_I\rangle,$$

where $m_I=I,\ I-1,\ \cdots,\ 1-I,\ -I$. An energy level diagram, for the case of $S=\frac{1}{2}$ and $I=\frac{1}{2}$, is shown in Fig. 2.

The Electron Spin Echo

In a two pulse spin-echo experiment a first 90° pulse excites the system by inducing spin transitions between the various spin levels. During the time τ between the first 90° and the second 180° pulse, let the initial wave function ψ_0 prepared after a 90° pulse change phase

[8] W. Marshall, Theoretical Physics Division, Atomic Energy Research Establishment (Harwell, Berkshire, England), Report No. AERE-T.P. 86, 1962 (unpublished).

[9] For simplicity we have assumed here that the anisotropic hyperfine interaction is of the same form and has the same axes as the classical dipolar interaction. ENDOR experiments to be described later indicate that the actual situation in $CaWO_4$ is less simple than this, particularly because lattice distortion can be involved as well. The use of a more general interaction Hamiltonian does not change the essential features of the echo amplitude calculation, although it will modify the values of the coefficients A and B introduced in Eq. (2).

[10] W. Low, in *Solid State Physics*, edited by F. Seitz and D. Turnbull (Academic Press Inc., New York, 1960), Suppl. 2, p. 52.

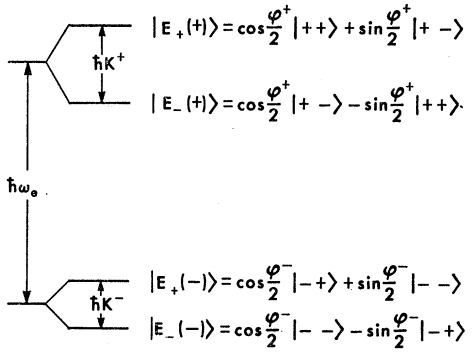

FIG. 2. Energy level diagram for dipolar coupled electron spin $S=\frac{1}{2}$ and nuclear spin $I=\frac{1}{2}$. The eigenstates are denoted by $|E_{mI}(m_S)\rangle$ where $+$ and $-$ correspond to m_I, m_S values of $+\frac{1}{2}$ and $-\frac{1}{2}$.

according to the transformation

$$\psi(t)=e^{i(\mp\omega_e+K^{\mp})t/2}\psi_0.$$

The 180° pulse at $t=\tau$ transforms $\psi(\tau)$ to $\psi(\tau+t_w)$ where t_w is the pulse width; and the wave function which contributes to the electron echo at $t=\tau$ after the second pulse is given by

$$\psi(\tau)=e^{i(\mp\omega_e+K^{\mp})\tau/2}e^{i(\pm\omega_e+K^{\pm})\tau/2}\psi_0=e^{i(K^{\pm}+K^{\mp})\tau}\psi_0,$$

which contains periods related to the nuclear Larmor frequencies K^+ and K^-.

The rigorous explicit expressions for the spin-echo envelope are conveniently obtained from the density matrix formalism. A simplification is introduced first by a transformation to the electron rotating frame Hamiltonian

$$\mathcal{H}_r=(\exp i\omega_e S_z t)\mathcal{H}\,(\exp -i\omega_e S_z t)=\mathcal{H}-\hbar\omega_e S_z, \quad (8)$$

which eliminates the electron Larmor frequency term in $\mathcal{H}$ given by Eq. (2). Prior to the 90° pulse the spin system is represented by an equilibrium density matrix in the high-temperature approximation as

$$\rho_0=\sum_{j=1}^{N}\mathcal{H}_j/kT\,\mathrm{Tr}1=\hbar\omega_e(\sum_{j=1}^{N}S_{zj}/kT\,\mathrm{Tr}1),$$

where the sum is taken over N electrons cm^{-3}, and the electron spin Zeeman energy dominates the contribution to ρ_0. In the calculations which follow, it will be understood that all spin operators S pertain to a sum over N electrons cm^{-3}, and I pertains to a total of nN nuclei, where there are n near nuclear neighbors about each isolated electron. The dipole-dipole coupling among nuclei is neglected. The time evolution of the density matrix is given by

$$\rho(t)=\mathcal{T}(t)\rho_0\mathcal{T}(t)^{-1}. \quad (9)$$

In the spin-echo experiment the Hamiltonian has two forms. In the absence of microwave pulses, $\mathcal{H}$ is given by Eq. (2), and when the pulses are applied the Hamiltonian becomes

$$\mathcal{H}(t)=\mathcal{H}+2\hbar\omega_1 S_y\cos\omega t, \quad (10)$$

where $2\hbar\omega_1=g\beta H_{rf}$; H_{rf} is the amplitude of the applied microwave field, and $2g\beta$ is the effective magnetic moment of the electron spin involved in transitions between the eigenstates of $\mathcal{H}$. In the representation given by Eq. (9), the transformation leading to Eq. (8) is applied to Eq. (10), and the secular Hamiltonian

$$\mathcal{H}_r'=\mathcal{H}_r+\hbar\omega_1 S_y\approx\hbar\omega_1 S_y \quad (11)$$

is used during microwave pulses. The experimental conditions $\omega\approx\omega_e$; $\omega_1\gg\omega_n$, A, B; and $\omega_e\gg\omega_n$, A, B will apply, and therefore $\mathcal{H}_r$ in Eq. (11) can be neglected during short microwave pulses. The transformation operator $\mathcal{T}(t)$ in Eq. (9) is a product of operators $\mathcal{T}_i(t)=\exp(i\mathcal{H}_r t/\hbar)$ or $\exp(i\mathcal{H}_r' t/\hbar)$, using the form of Hamiltonians in Eq. (8) or (11), depending upon whether the microwave pulses are off or on respectively during a given time segment. Therefore,

$$\mathcal{T}(t)=\mathcal{T}_0(t)\mathcal{T}_1(\theta_2)\mathcal{T}_0(\tau)\mathcal{T}_1(\theta_1), \quad (12)$$

where

$$\mathcal{T}_0(t)=\exp(-i\mathcal{H}_r t/\hbar), \quad (13)$$

$$\left.\begin{aligned}\mathcal{T}_1(\theta_1)&=\exp(-iS_y\pi/2),\\ \mathcal{T}_1(\theta_2)&=\exp(-iS_y\pi),\end{aligned}\right\} \quad (14)$$

with $\omega_1 t_w=\pi/2=\theta_1$ and $2\omega_1 t_w=\pi=\theta_2$. The observed electron echo signal with its maximum at $t=\tau$ is given by

$$V(t)=Ng\beta\,\mathrm{Tr}\{S_+\rho(t)\} \quad (15)$$

where $S_+=S_x=iS_y$. The trace is taken over both electron and nuclear spin orientations. From Eq. (9), using Eqs. (12), (13), and (14),

$$\begin{aligned}\rho(t)=&\exp -i\{(AS_z-\omega_n)I_z+BS_zI_x\}t\\ &\times\exp+i\{(AS_z+\omega_n)I_z+BS_zI_x\}\tau\\ &\times\hbar\omega_e S_x/(kT\,\mathrm{Tr}1)\\ &\times\exp -i\{(AS_z+\omega_n)I_z+BS_zI_x\}\tau\\ &\times\exp+i\{(AS_z-\omega_n)I_z+BS_zI_x\}t. \quad (16)\end{aligned}$$

Details of the evaluation of the trace stated by Eq. (15) are given in the Appendix. The echo signal maximum at $t=\tau$ after the second pulse for $S=\frac{1}{2}$ and $I=\frac{1}{2}$ is

$$V(\tau)=V(0)\left[1-2\left(\frac{B\omega_n}{K^+K^-}\right)^2\times\sin^2\left(\frac{K^+\tau}{2}\right)\sin^2\left(\frac{K^-\tau}{2}\right)\right], \quad (17)$$

where $V(0)$ is the echo signal amplitude in the absence of nuclear coupling.

The signal $V(\tau)$ of Eq. (17) as it stands refers to the coupling between isolated electron-nucleus pairs which are all identical with regard to the orientation param-

eters defined in the Hamiltonian given by Eq. (2). Assuming identical isolated electron-nucleus pair interactions, if the nuclei have several natural isotope fractions p, the total signal for a given electron-nuclear pair orientation is given by a linear superposition of the signals from each distinct nuclear isotope-electron pair weighted by the natural isotopic abundance. For example, if only two isotopes exist such that p is the fraction of nuclei with spin $I\neq 0$ and $1-p$ is the fraction of nuclei with spin $I=0$, then the signal voltage for the pair interaction for the ith nuclear neighbor is

$$V_i(\tau)=V_{I=0}(\tau)(1-p)+V_I(\tau)p$$
$$=V(0)\left[1-2p\left(\frac{B_i\omega_{ni}}{K_i^+K_i^-}\right)^2\times\sin^2\left(\frac{K_i^+\tau}{2}\right)\sin^2\left(\frac{K_i^-\tau}{2}\right)\right], \quad (18)$$

where $V_I(\tau)$ is equivalent to $V(\tau)$ given by Eq. (17) and $V_{I=0}(1-p)=V(0)(1-p)$. When the nuclei are distributed over many possible neighboring lattice sites $i=1$ to n, about a single electron spin, where each nucleus interacts independently but simultaneously with the electron, the number of different ways the various nuclear sites can be occupied is manifested in a total signal

$$V(\tau)=\prod_{i=1}^{n} V_i(\tau). \quad (19)$$

In our special case, application of Eq. (18) gives

$$V(\tau)=V(0)\prod_{i=1}^{n}\left[1-2p\left(\frac{B_i\omega_{ni}}{K_i^+K_i^-}\right)^2\times\sin^2\left(\frac{K_i^+\tau}{2}\right)\sin^2\left(\frac{K_i^-\tau}{2}\right)\right]. \quad (20)$$

From the formalism developed for the electron spin echo in the Appendix, the free precession signal after a single 90° pulse is given by

$$V(t)=\frac{V(0)}{2}\prod_{i=1}^{n}\left\{\cos\left(\frac{K_i^++K_i^-}{2}\right)t+\sin\left(\frac{K_i^+-K_i^-}{2}\right)t+\left[\left(\frac{A_i^2+B_i^2}{4}-\omega_{ni}^2\right)\Big/(K_i^+K_i^-)\right]\times\left[\cos\left(\frac{K_i^++K_i^-}{2}\right)t-\sin\left(\frac{K_i^+-K_i^-}{2}\right)t\right]\right\}. \quad (21)$$

For $B_i=0$, $K_i^{\pm}=(A_i/2)\pm\omega_{ni}$, and then

$$V(t)=V(0)\prod_{i=1}^{n}\cos A_i t,$$

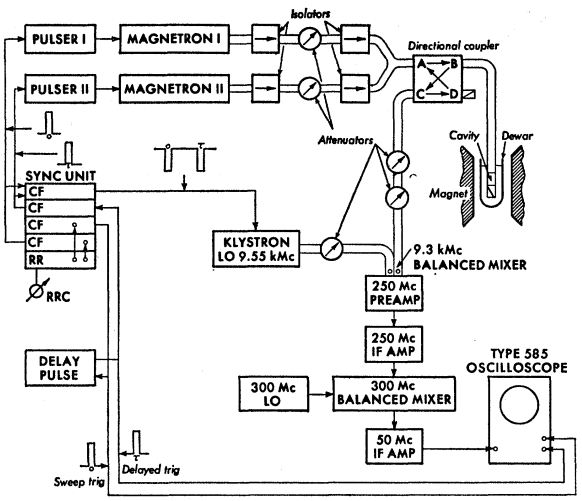

FIG. 3. Block diagram of the two-pulse electron-spin-echo apparatus operating at 9.3 kMc/sec (X band). CF≡cathode follower; RR≡repetition rate oscillator; RRC≡repetition rate oscillator control; LO≡local oscillator.

which is the free precession signal from an inhomogeneously broadened spin system.[11]

III. ECHO ENVELOPE MEASUREMENTS

Ce^{3+} in $CaWO_4$

The X-band spin-echo spectrometer used in the experiment[4] produces two 120-W microwave pulses of 0.1 μsec duration separated by a time τ. The apparatus is similar to that developed by Kaplan,[3] but is modified in several respects. A block diagram is given in Fig. 3. Two negative voltage pulses are applied, coincident with the magnetron pulses, on the repeller of the receiver local oscillator klystron so that the receiver is detuned during the time that the magnetrons are radiating, which therefore protects the receiver from the high power radiation of the magnetrons. The over-all bandwidth of the receiver is about 70 Mc/sec.

A single crystal of $CaWO_4$ containing about 0.01% Ce^{3+} ions by weight is placed in a low-Q cavity cooled to liquid-helium temperatures. The crystal symmetry of $CaWO_4$ is tetragonal,[12] and it is assumed that the Ce^{3+} ions are located in Ca^{2+} sites with the creation of Ca^{2+} vacancies in order to provide for charge compensation. The magnetic field H_0 is oriented at an angle θ_0 with respect to the crystal C axis, and at an angle φ_0 with respect to the crystal A axis, where φ_0 is taken arbitrarily as zero in defining Eq. (2). For φ_0 finite, then φ_I in Eq. (2) must be replaced by $\varphi_I-\varphi_0$. A 90°–180° microwave pulse pair separated by a time τ is applied to the sample, with H_{rf} perpendicular to H_0. When the EPR resonance condition is fulfilled, an echo pulse is observed at a time τ after the second microwave

[11] I. Lowe and R. E. Norberg, Phys. Rev. **107**, 46 (1957).
[12] A. Zalkin and D. H. Templeton, J. Chem. Phys. **40**, 501 (1964).

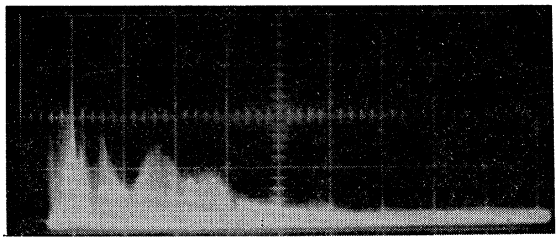

FIG. 4. Multiple oscilloscope sweep exposures of electron spin echoes from Ce^{3+} in $CaWO_4$. This particular echo envelope measurement pertains to the plot given by Fig. 6(a). The sweep rate is 1 μsec per graticule division. The 180° pulse occurs at the left of the sweep on the 1 μsec time point.

pulse. Since the oscilloscope sweep is triggered by the second pulse, the oscilloscope displays the second microwave pulse at the start of the sweep and the echo pulse appears at a time τ later. In Fig. 4, a representative photograph of the sweep is shown of the echo envelope, which is obtained by multiple exposure of the oscilloscope display, where τ is changed to a larger value of each exposure. The data from the photograph are then transferred to semilog paper and normalized to compensate for an over-all echo decay function approximated by $\exp(-2\tau/T_2)$. A $T_2\sim 16$ μsec is inferred by measurements of the echo envelope decay for orientations in which the beat pattern was not marked. A 7090 computer was programmed to compute the echo signal $V(\tau)$ given by Eq. (20). The computer program utilizes the four nearest tungsten neighbors, the four next-nearest neighbors, and two next neighbors along the C axis as shown in Fig. 5. Inclusion of farther out nearest neighbors proved in later analysis to have less than 2% effect on the calculation which includes the total above of 10 neighbors. The assumption that the electron spin is at a point instead of being distributed about the Ce^{3+} site introduces an error no more than a few percent. The known values of $g_{\parallel}$, $g_{\perp}$, percent abundance p, nuclear gyromagnetic ratio γ_n, and the effective lattice spacings r(Å) are given in Table I, where $r(\text{Å})=r\rho^{-1/3}$, and r, θ_I, φ_I are the lattice values. Computations of Eq. (20) are made for φ_0 fixed at 20° and for 10-deg increments in the value of θ_0 from 0 to 90°. The comparison of experimental and theoretical spin echo envelopes are given in Figs. 6(a) and 6(b).

To obtain the best least squares fit to the data, the dipolar correction factor ρ is adjusted to a value $\rho=4.0\pm0.5$, and the isotropic hyperfine factor α is fitted at $\alpha=(0.0\pm0.1)\times gg_n\beta_n\beta/r^3$, where these parameters are introduced in Eq. (1). The fact that the pseudo dipolar coupling constant $\rho-1$ may vary from ligand site to ligand site is neglected in our calculation. From a careful procedure of curve fitting, it is found that variations in α alter the frequency of modulation much more than the depth of modulation. In contrast, the parameter $\rho-1$ affects the depth of modulation more than the frequency of modulation. The error in ρ is attributed in part to the rather imprecise procedure of

TABLE I. Parameters for electron-spin-echo envelope modulation curve computations. The effective lattice distance is $r(\text{Å})=r\rho^{-1/3}$, where r, θ_I, and φ_I are lattice values. For Ce^{3+} in $CaWO_4$, $\rho\approx4$ and $\alpha\approx0$; for Ce^{3+} in CaF_2, $\rho\approx8$ and $\alpha\approx0$.

$CaWO_4$			
Ce^{3+}	W sites		
$g_{\parallel}=2.92$	θ_I	Φ_I	r(Å)
$g_{\perp}=1.43$	90.0	45.0	2.30
$\gamma_n=0.175$ Mc/(sec kG)	90.0	135.0	2.30
$p=0.14$	90.0	225.0	2.30
	90.0	315.0	2.30
	42.6	90.0	2.36
	42.6	270.0	2.36
	137.4	00.0	2.36
	137.4	180.0	2.36
	00.0	00.0	3.48
	180.0	00.0	3.48
CaF_2			
Ce^{3+}	F sites		
$g_{\parallel}=3.04$	θ_I	Φ_I	r(Å)
$g_{\perp}=1.40$	45.0	45.0	2.36
$\gamma_n=4.006$ Mc/(sec kG)	45.0	135.0	2.36
$p=1.00$	45.0	225.0	2.36
	45.0	315.0	2.36
	135.0	45.0	2.36
	135.0	135.0	2.36
	135.0	225.0	2.36
	135.0	315.0	2.36

normalizing the echo envelope to correct for the decay due to electron-electron dipolar interactions. The T_2 dependence upon g as a function of θ was not included. This decay correction function cannot be precisely determined because neighboring tungsten nuclei influence the electron echo signal unavoidably, even for crystal orientations where the modulation is at a minimum, and prevent a clear measure of the monotonic decay function in the absence of modulation (see also footnote 9).

Lattice distortions arising from the charge-compensating mechanism can be inferred from the anisotropy of the electron paramagnetic resonance spectrum given in terms of the g tensor. As discussed by Mims and Klein,[13] the Ce^{3+} sites which are distorted by

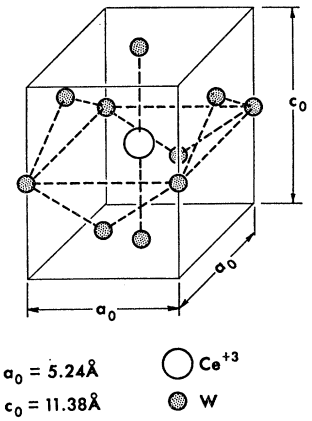

FIG. 5. Crystal lattice configuration of tungsten atoms W about the Ce^{3+} ion, where Ce^{3+} replaces Ca^{2+} in the normal $CaWO_4$ lattice. The C crystalline axis passes through the Ce^{3+} site parallel to $\mathbf{c}_0$, and the A crystalline axis passes through the Ce^{3+} site parallel to either of the $\mathbf{a}_0$ directions.

[13] M. P. Klein and W. B. Mims, Bull. Am. Phys. Soc. 7, 625 (1962).

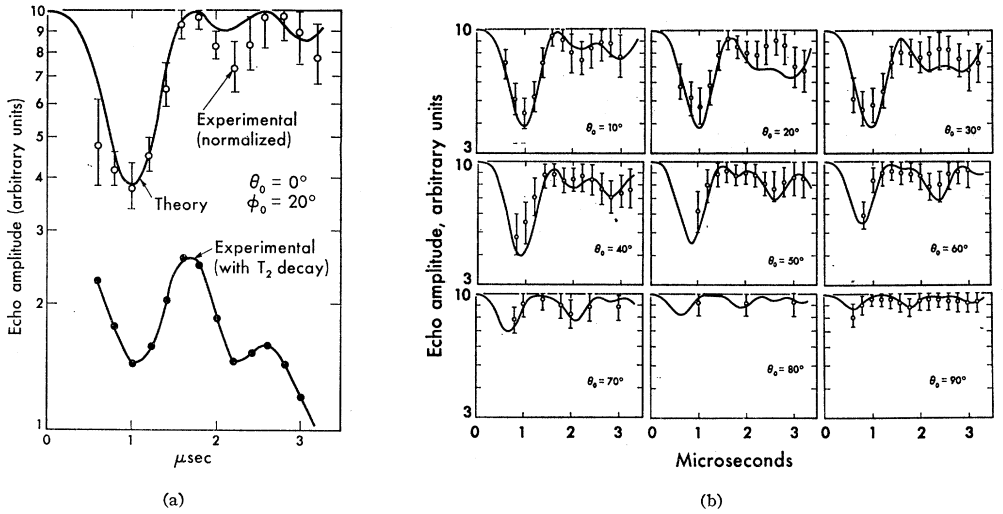

FIG. 6. (a) Semilog plot of electron-spin-echo amplitude from Ce^{3+} in $CaWO_4$ versus time τ after the 180° pulse for $\theta_0=0°$ and $\varphi_0=20°$. Normalized and measured plots are shown. The over-all monotonic decay time T_2 is determined from the echo envelope plot at $\theta_0=80°$ as representative for all values of θ_0. (b) Normalized semilog plots of electron-spin-echo amplitude versus time τ after the 180° pulse for 10° increments of θ_0. For all plots, $\varphi_0=20°$. The solid plots are from theory and the points are from experiment.

neighboring vacancies are separated in frequency from the axial sites in $CaWO_4$. The data here refer to Ce^{3+} at axial sites for which this gross distortion is absent. It is, however, possible that the substitution of Ce^{3+} for Ca^{2+} causes changes in the length r and in the angles θ_I and φ_I. Provided that S_4 symmetry is preserved at the Ce^{3+} site, these distortions will not be apparent from the g tensor, although they will change the strength, and may modify the axes of the dipolar interaction. It is likely, moreover, that any pseudodipolar interaction will be characterized by the axes of the WO_4 group rather than by the axes joining Ce and W nuclei. We have not attempted to take all these possibilities into account in fitting the echo envelopes, nor can we estimate the relative importance of lattice distortions and pseudodipolar contributions in determining the magnitude of the over-all interaction. The parameter ρ should rather be taken as an approximate measure of the enhancement of the dipolar interaction due to one or both causes.

Preliminary ENDOR-type experiments utilizing a pulse stimulated echo method have been performed by one of us (WBM) on Ce^{3+} in $CaWO_4$ at $\omega_e=9.42$ Gc/sec. The four nearest nuclei (corresponding to those at $\theta_I=42.6°$ and 137.4° in Table I) have nuclear resonance transitions $K^{\pm}/2\pi$ of 605 kc/sec and 320 kc/sec. From the echo modulation data we infer values of $K^{\pm}/2\pi=580$ and 390 kc/sec, respectively, using $\rho=4.0$. ENDOR measurements of the other set of nearest tungsten nuclei (those at $\theta_I=90°$ in Table I) have shown that the interaction is similar in magnitude, although of course different in orientation, to that for the above first set. ENDOR measurements of the two nuclei with $\theta_I=0°$ and 180° indicate parameter values of $|A|\approx 50$ kc/sec and $|B|=0$ kc/sec whereas from the echo data, assuming $\rho=4.0$, we should infer $|A|\approx 200$ kc/sec and $|B|=0$ kc/sec. This indicates that ρ is considerably smaller for these sites and is close to unity. It may be noted that the oxygen atoms belonging to the WO_4 groups centered on these nuclei are not amongst the eight nearest neighbors of the Ce^{3+} ion, and that the pseudodipolar interaction may in this case be expected to be considerably smaller.

Ce^{3+} in CaF_2

The symmetry of CaF_2 is cubic and has the characteristic flourite arrangement, where the 0.01% Ce^{3+} ions appear to substitute for Ca^{2+} sites,[14] and the flourine nuclear moments cause the electron echo modulation. A computer calculation similar to the one described above was also performed for CaF_2. The theoretical plot of Eq. (20), using data in Table I, is shown in Fig. 7. A single echo envelope experimental measure is shown. Since the flourine nuclei with spin $I=\frac{1}{2}$ are 100% abundant, the echo envelope modulation is very deep. The modulation beat periods are generally shorter than the width of the echo signal itself so that accurate details of the beat pattern due to echo maxima are obscured if analyzed directly from a superposition of photographs of the echo amplitude as a function of τ. The measurements, in fact, could not be made with the pulse width condition $t_w \ll 2\pi/\omega_n$, necessary in the theory of the experiment, but rather with the pulse condition $t_w \sim 2\pi/\omega_n$ because of technical limitations upon the microwave power and pulse widths that would be

[14] J. M. Baker, W. Hayes, and D. A. Jones, Proc. Phys. Soc. (London) **73**, 942 (1959).

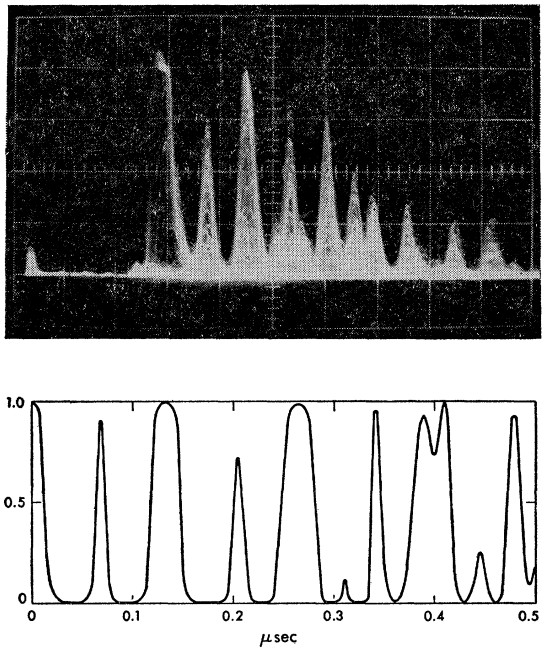

FIG. 7. Experimental oscilloscope (above) and theoretical (below) plots of the electron spin echo envelope of Ce^{3+} in CaF_2. The sweep speed is 0.1 μsec per graticule division. The 180° pulse occurs at the beginning of the trace. Receiver blocking after the pulse occurs for about 0.25 μsec.

produced. No attempt was made to compare in detail the echo pattern, as predicted by the theory, to the actual echo envelope measurements. Because of the microwave pulse condition $t_w \approx (\gamma_e H_{rf})^{-1} \approx 1/\omega_n$, the F nuclei undergo a cross relaxation with the electrons imposed by a double resonance condition[15] $\gamma_n H_0 \approx \gamma_e H_{rf}$; i.e., the Zeeman splitting of the electron system in the frame of reference rotating at frequency ω_e becomes comparable to the Zeeman splitting of the nuclei in the laboratory frame. This effect is excluded by our theory. However, in spite of this discrepancy in pulse conditions required by the echo envelope and the actual experiment in this case, the observed Ce^{3+} echo modulation in CaF_2 has a character similar to the theoretical modulation curve.

IV. CONCLUSIONS

The detailed structure of electron spin-echo modulation due to neighboring ligand nuclei provides information about dipolar and hyperfine interactions with paramagnetic ions. In the case of Ce^{3+} in $CaWO_4$, if it is assumed that the lattice parameters relating Ce^{3+} to tungsten nuclei are not distorted from the values given for the pure $CaWO_4$ crystal, the direct dipole-dipole interaction between electron and nucleus appears to be enhanced by a pseudodipolar interaction, at most, about 4 times as large as the direct interaction. It is difficult, if not impossible, to infer the crystal symmetry of the ligands and the directional dependance of the pseudodipolar interaction from the structure of the echo modulations. The ENDOR method picks out the discrete NMR transitions that contribute to the echo modulations, whereas the pulse method integrates the effect of different transitions of all close neighboring nuclei. However, the ENDOR technique requires that the EPR saturation be sufficient to burn and maintain a hole in the inhomogeneously broadened EPR line, where the hole in the spectrum is not filled up at an overwhelming rate by the counteracting process of electron spin-spin diffusion in the frequency spectrum. In cases where such diffusion rates are so rapid as to prevent observations of ENDOR transitions, the spin-echo method, on the other hand, does succeed if the EPR line is narrow enough so that it can be excited reasonably completely throughout its frequency spectrum by short intense microwave pulses. In this way, an echo of sufficient amplitude can be observed in times short compared to times in which complete echo-envelope attenuation is caused by electron-spin diffusion.

When electron spins with $S>\frac{1}{2}$ are dipolar coupled to a nuclear spin I, another Hamiltonian term of the form $D[S_z^2-(S+1)/3]$ can arise due to axial symmetry of the crystal field which produces a zero magnetic-field splitting corresponding to the parameter D. The exact theoretical treatment of the echo modulation in this case is more complicated than for the case $D=0$ given in this paper. The added DS_z^2 term shifts the Zeeman energy levels so that generally the EPR resonance condition can only be fulfilled between two levels at a time. Each level, of course, is split in turn by dipolar coupling to the ligand nuclei, but an added complication results in that the electron spin states are now generally admixtures; namely, they are no longer pure states even in the absence of coupling with neighboring nuclear moments. Therefore, the axial crystal field causes the electron spin to be quantized not along the applied magnetic field H_0 axis, but along some other axis. This tilting of the electron-spin quantization axis can produce a dipolar field which is not aligned with the applied field at the ligand nucleus site even when the nucleus with $I=\frac{1}{2}$ is quantized along an H_0 direction which is perpendicular to the plane containing the nuclear and electron spins. If the nucleus has $I>\frac{1}{2}$, as in the case for $Al^{27}(I=\frac{5}{2})$ in Cr^{3+} doped Al_2O_3 (ruby), the Cr^{3+} spin-echo envelope is not only complicated by the DS_z^2 term discussed above but also includes the effect that the Al^{27} nuclei themselves can be aligned in complicated directions determined by the nuclear quadrupole interactions[16] if they are comparable to the nuclear magnetic interaction μH_0.

An extension of the theory of the echo-envelope analysis to the case where the pulse angle conditions deviate from the ideal 90°–180° sequence shows that

[15] S. R. Hartmann and E. L. Hahn, Phys. Rev. **128**, 2042 (1962).

[16] R. V. Pound, Phys. Rev. **79**, 685 (1950).

the shape of the echo envelope is identical to the ideal case except that the amplitude of the over-all envelope signal is reduced by a common factor. This is the case when the EPR line is so broad that all the spin packets are not subjected to 90°–180° orientations when the pulse power is inadequate to excite the entire spin spectrum.

ACKNOWLEDGMENTS

The authors wish to thank Dr. D. E. Kaplan for many helpful, stimulating discussions, his advice in the construction of our apparatus, and for generously informing us of some of the earlier results of his spin-echo experiments. Helpful discussions with Professor W. A. Nierenberg concerning rotation transformations are gratefully acknowledged.

APPENDIX

The echo envelope is calculated from the relation

$$V_i(t,\tau)=g\beta\,\mathrm{Tr}\{\rho(t,\tau)S_+\}$$

$$=g\beta\sum_{m_{Sj}=-S_j}^{Sj}\sum_{m_{Ij}=-I_{ji}}^{Iji}\langle m_S,m_I|\rho(t,\tau)S_+|m_S,m_I\rangle, \quad \text{(A1)}$$

where N identical but isolated electron-nucleus pairs are interacting. Products of electron-nucleus spin states for each jth pair over the entire ensemble are represented as

$$m_S,\ m_I\equiv\sum_{j=1}^{N} m_{Sj}m_{Iji}.$$

The nuclear state m_{Iji} pertains to the ith nucleus belonging to a total of n nuclear neighbors surrounding the jth electron, where the ith neighbor has the particular coordinates r_{ij}, θ_{ij}, and φ_{ij} with respect to the electron. Spin variables which appear in operators of the Hamiltonian [Eq. (1)] and in ρ of Eq. (9) of the text are given by

$$\mathbf{S}=\sum_{j=1}^{N}\mathbf{S}_j \quad \text{and} \quad \mathbf{I}=\sum_{j=1}^{N}\sum_{i=1}^{n}\mathbf{I}_{ji}.$$

Assuming that all nuclei are of a given 100% abundant isotopic species, the total echo signal, taking into account n nuclear neighbors, is given by

$$V(t,\tau)=\prod_{i=1}^{n}V_i(t,\tau).$$

Equation (A1) may be written as

$$V_i(t,\tau)=g\beta\sum_{m_{Sj}=-S_j}^{Sj}\{\langle m_S+1|S_+|m_S\rangle \times\sum_{m_{Ij}=-I_j}^{Ij}\langle m_S,m_I|\rho(t,\tau)|m_S,m_I\rangle\}. \quad \text{(A2)}$$

The summation over j in Eq. (A2) is now carried out, and $\rho(t,\tau)$ from Eq. (16) is substituted. Since all electrons and nuclei are taken to have the same S_j and I_j, respectively, the notation S, I, m_S, and m_I will henceforth pertain to the single spins. Therefore Eq. (A2) becomes

$$V_i(t,\tau)=\frac{Ng\beta\hbar\omega_e}{(2S+1)kT}\sum_{m_S=-S}^{S}\{\langle m_S+1|S_+^2|m\rangle G(m_S,t,\tau)\}, \quad \text{(A3)}$$

where

$$G(m_S,t,\tau)=(2I+1)^{-1}\sum_{m_I=-I}^{I}\langle m_I|\exp-i\{(A_im_I-\omega_n)I_z+B_im_SI_x\}t\exp+i\{(A_im_S+\omega_n)I_z+B_im_SI_x\}\tau$$

$$\times\exp+i\{[A_i(m_S+1)+\omega_n]I_z+B_i(m_S+1)I_x\}\tau\exp-i\{[A_i(m_S+1)-\omega_n]I_z+B_i(m_S+1)I_x\}t|m_I\rangle. \quad \text{(A4)}$$

The function $G(m_S,t,\tau)$ is evaluated by expressing the exponential functions in terms of rotation operators having known matrix elements. For example:

$$\exp i\{(Am_S+\omega_n)I_z+Bm_SI_x\}\tau=\exp i(e^{-i\varphi I_y}KI_ze^{+i\varphi I_y})\tau=\exp(-i\varphi I_y)\exp(i-KI_z\tau)\exp(i\varphi I_y),$$

where $\tan\varphi=Bm_S/(\omega_n+Am_S)$ and $K=[(\omega_n+Am_S)^2+(Bm_S)^2]^{1/2}$. The subscript i is omitted for simplicity of notation. Transformation of each exponential term in Eq. (A4) in this way gives

$$G(m_S,t,\tau)=(2I+1)^{-1}\sum_{m_I=-I}^{I}\langle m_I|\exp(-i\varphi_2^-I_y)\exp(-iK_2^-I_zt)\exp(i\varphi_2^-I_y)\exp(-i\varphi_1^-I_y)\exp(-iK_1^-I_z\tau)\exp(i\varphi_1^-I_y)$$

$$\times\exp(-i\varphi_1^+I_y)\exp(iK_1^+I_z\tau)\exp(i\varphi_1^+I_y)\exp(-i\varphi_2^+I_y)\exp(iK_2^+I_zt)\exp(i\varphi_2^+I_y)|m_I\rangle, \quad \text{(A5)}$$

where

$$\begin{aligned}
K_2^-\cos\varphi_2^- &= -\omega_n+Am_S, & K_1^+\cos\varphi_1^+ &= -\omega_n-A(m_S+1),\\
K_2^-\sin\varphi_2^- &= Bm_S, & K_1^+\sin\varphi_1^+ &= -B(m_S+1),\\
K_1^-\cos\varphi_1^- &= \omega_n-Am_S, & K_2^+\cos\varphi_2^+ &= -\omega_n+A(m_S+1),\\
K_1^-\sin\varphi_1^- &= Bm_S, & K_2^+\sin\varphi_2^+ &= B(m_S+1).
\end{aligned} \quad \text{(A6)}$$

Equation (A5) can be further simplified by combining adjacent $\exp(i\varphi I_y)$ terms and combining the last exponential operator with the first one as can be done in a trace. Therefore,

$$G(m_S,t,\tau)=(2I+1)^{-1}\sum_{m_I=-I}^{I}\langle m_I|\exp\{i(\varphi_2^+-\varphi_2^-)I_y\}\exp\{-iK_2^-I_zt\}\exp\{i(\varphi_2^--\varphi_1^-)I_y\}\exp\{-iK_1^-I_z\tau\}$$
$$\times\exp\{i(\varphi_1^--\varphi_1^+)I_y\}\exp\{+iK_1^+I_z\tau\}\exp\{i(\varphi_1^+-\varphi_2^+)I_y\}\exp\{+iK_2^+I_zt\}|m_I\rangle. \quad \text{(A7)}$$

Explicit formulas are given by Edmonds[17] for the matrix elements of exponential operators involving I_y, I_z, and the rotation angles α, β:

$$\langle m|\exp(i\alpha I_y)|m'\rangle\equiv d_{mm'}{}^{(I)}(\alpha)=\sum_\sigma\binom{I+m}{I-m'-\sigma}\binom{I-m}{\sigma}(-1)^{I-m'-\sigma}\left[\cos\frac{\alpha}{2}\right]^{2\sigma+m'+m}\left[\sin\frac{\alpha}{2}\right]^{2I-2\sigma-m'-m};$$

and $\langle m|\exp(i\beta I_z)|m'\rangle=\sigma_{mm'}\exp(im'\beta)$. For any electron spin S and nuclear spin I the final form for $G(m_S,t,\tau)$ is

$$G(m_S,t,\tau)=(2I+1)^{-1}\sum_{m,m',m'',m'''=-I}^{I}d_{mm'}{}^{(I)}(\varphi_2^+-\varphi_2^-)d_{m'm''}{}^{(I)}(\varphi_2^--\varphi_1^-)$$
$$\times d_{m''m'''}{}^{(I)}(\varphi_1^--\varphi_1^+)d_{m'''m}{}^{(I)}(\varphi_1^+-\varphi_2^+)\exp(-iX), \quad \text{(A8)}$$

where

$$X=(K_2^-m'-K_2^+m)t+(K_1^-m''-K_1^+m''')\tau.$$

For the case $S=\frac{1}{2}$, $I=\frac{1}{2}$, the relations (A6) simplify to

$$K_2^-\cos\varphi_2^-=-\omega_n-\tfrac{1}{2}A=K_1^+\cos\varphi_1^+,$$
$$K_2^-\sin\varphi_2^-=-B/2=K_1^+\sin\varphi_1^+,$$
$$K_1^-\cos\varphi_1^-=-\omega_n+\tfrac{1}{2}A=K_2^+\cos\varphi_2^+,$$
$$K_1^-\sin\varphi_1^-=B/2=K_2^+\sin\varphi_2^+,$$

where we write

$$K^+=K_2^-=K_1^+=[(\omega_n+\tfrac{1}{2}A)^2+\tfrac{1}{4}B^2]^{1/2},$$

and

$$K^-=K_1^-=K_2^+=[(\omega_n-\tfrac{1}{2}A)^2+\tfrac{1}{4}B^2]^{1/2}.$$

Note also that

$$\varphi_2^+-\varphi_2^-=\varphi_2^+-\varphi_1^+=\delta,$$
$$\varphi_2^--\varphi_1^-=\varphi_1^+-\varphi_2^+=-\delta,$$
$$\varphi_1^--\varphi_1^+=\varphi_2^+-\varphi_1^+=\delta;$$

and

$$X=K^+(m't-m'''\tau)-K^-(m''\tau-mt).$$

The matrices of the operators for $I=\frac{1}{2}$ are

$$\exp(i\alpha I_y)\equiv\begin{pmatrix}\cos\alpha/2 & \sin\alpha/2\\ -\sin\alpha/2 & \cos\alpha/2\end{pmatrix};\qquad \exp(i\beta I_z)\equiv\begin{pmatrix}\exp i\beta/2 & 0\\ 0 & \exp -i\beta/2\end{pmatrix}.$$

After matrix multiplication,

$$G(\tfrac{1}{2},t,\tau)=\left(\cos^4\frac{\delta}{2}\right)\cos\left[\frac{(K^+-K^-)(t-\tau)}{2}\right]+\left(\sin^4\frac{\delta}{2}\right)\cos\left[\frac{(K^++K^-)(t-\tau)}{2}\right]+2\sin^2\delta\left\{\cos\left[\frac{K^+(t+\tau)}{2}\right]\cos\left[\frac{K^-(t-\tau)}{2}\right]\right.$$
$$\left.+\cos\left[\frac{K^-(t+\tau)}{2}\right]\cos\left[\frac{K^+(t-\tau)}{2}\right]-\cos\left[\frac{K^+(t+\tau)}{2}\right]\cos\left[\frac{K^-(t+\tau)}{2}\right]\right\}. \quad \text{(A9)}$$

---

[17] A. R. Edmonds, *Angular Momentum in Quantum Mechanics* (Princeton University Press, Princeton, New Jersey, 1957), Chap. 4, pp. 53–57.

Upon reinstating the subscript i and evaluating the echo envelope function at $t=\tau$, substitution of Eq. (A9) into Eq. (A3) gives

$$V_i(\tau)=V(0)\left[1-2\sin^2\delta_i\sin^2\left(\frac{K_i^+\tau}{2}\right)\sin^2\left(\frac{K_i^-\tau}{2}\right)\right]$$

$$=V(0)\left[1-2\left(\frac{B_i\omega_n}{K_i^+K_i^-}\right)^2\sin^2\left(\frac{K_i^+\tau}{2}\right)\sin^2\left(\frac{K_i^-\tau}{2}\right)\right],$$

where $V(0)=Ng\beta\hbar S(S+1)\omega_e/3kT$.

PHYSICAL REVIEW VOLUME 137, NUMBER 1A 4 JANUARY 1965

Paramagnetic Resonance Linewidths in Some Rare-Earth Double Nitrates

P. L. Scott*
Clarendon Laboratory, Oxford, England

H. J. Stapleton†
Department of Physics, University of Illinois, Urbana, Illinois

AND

C. Wainstein‡
Department of Physics, University of California, Berkeley, California

(Received 30 August 1963; revised manuscript received 17 August 1964)

We have measured the paramagnetic resonance linewidth δH at microwave frequencies for the three trivalent rare-earth ions Ce, Nd, and Sm present in small concentrations in $La_2Mg_3(NO_3)_{12}\cdot 24H_2O$. The linewidths appear to be strongly dependent upon the angle θ between the c axis of the crystal and the magnetic field, and in most cases the observed linewidths seem to be reasonably well explained by a simple theory which assumes a spatial distribution of paramagnetic resonance g values throughout the crystal.

I. EXPERIMENTAL APPARATUS AND PROCEDURES

We have measured the angular dependence of the paramagnetic resonance linewidth of trivalent cerium, neodymium, and samarium in a host matrix of lanthanum magnesium nitrate. The measurements were made in the liquid helium temperature range at frequencies around 9 kMc/sec, 23 kMc/sec, and 36 kMc/sec. Four different microwave spectrometers were used, each being a simple transmission or reflection system. The derivative peak-to-peak linewidth was measured as a function of the angle θ between the magnetic field H and the crystalline c axis. The crystals were grown from a saturated aqueous solution in a desiccator at 0°C, the high-purity rare-earth salts being obtained from the Lindsay Chemical Company. The crystals used were clear and visually free from imperfections. Concentrations of paramagnetic rare-earth ions ranged from approximately 0.003 to 0.2 at. %. In all cases, measurements were made on the single resonance line arising from the even isotopes.

The measurements on the Sm-doped crystal were made for a single crystal only, weighing approximately 100 mg, and at the single frequency $\nu=9.25$ kMc/sec. The relatively small g factors of the Sm ion combined with the limit on the strength of our magnetic field prevented us from making measurements at higher frequencies.

Where measurements were made for the same ion at different frequencies, the same sample was used for all frequencies, and the angle of rotation about the c axis was kept unchanged.

II. THEORY AND EXPERIMENTAL RESULTS

Of the several possible factors contributing to the width of a paramagnetic resonance line, we consider only two: first, the width caused by the interaction of the paramagnetic ion with the surrounding nuclei; and second, a possible spatial distribution of g values throughout the crystal, perhaps caused by lattice strains. Lattice strains as a contribution to paramagnetic resonance linewidths have also been considered by

* National Science Foundation Postdoctoral Fellow. Present address: Department of Physics, Stanford University, Stanford, California.
† Alfred P. Sloan Research Fellow.
‡ Fellow of Consejo Nacional de Investigaciones Cientificas y Tecnicas, Argentina. Now at Universidad Nacional de La Plata, La Plata, Argentina.

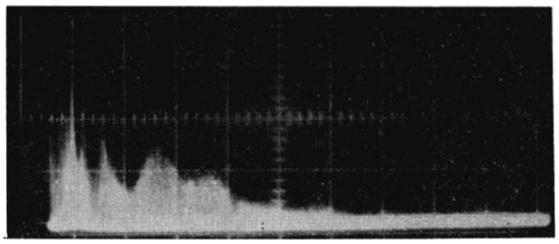

FIG. 4. Multiple oscilloscope sweep exposures of electron spin echoes from Ce^{3+} in $CaWO_4$. This particular echo envelope measurement pertains to the plot given by Fig. 6(a). The sweep rate is 1 μsec per graticule division. The 180° pulse occurs at the left of the sweep on the 1 μsec time point.

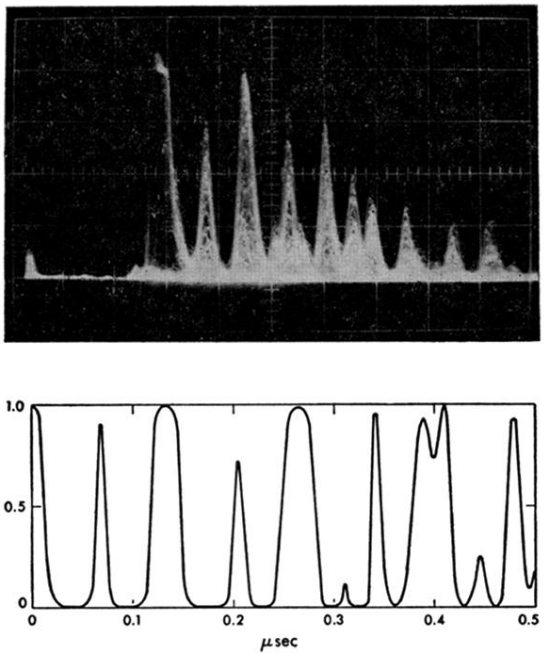

FIG. 7. Experimental oscilloscope (above) and theoretical (below) plots of the electron spin echo envelope of Ce^{3+} in CaF_2. The sweep speed is 0.1 μsec per graticule division. The 180° pulse occurs at the beginning of the trace. Receiver blocking after the pulse occurs for about 0.25 μsec.